Cancer Nanotechnology

RESEARCH Open Access

A combined miR-34a and arsenic trioxide nanodrug delivery system for synergistic inhibition of HCC progression after microwave ablation

Jian Hu[1,2*], Wenceng Pei[4], Zhenyou Jiang[1,3*] and Zihuang Li[1*]

*Correspondence: hujian@jnu.edu.cn; tjzhy@jnu.edu.cn; lizihuang2006@126.com
[1] Department of Oncology Radiotherapy, The Second Clinical Medical College, Jinan University (Shenzhen People's Hospital), Shenzhen 518020, China
Full list of author information is available at the end of the article

Abstract

Background: Microwave ablation (MWA) has become an alternative treatment for unresectable hepatocellular carcinoma (HCC), but it does not eliminate the risk of recurrence and metastasis after treatment. Recent studies have demonstrated that miR-34a presents decreased gene expression in residual tumours after ablation therapy and can increase the therapeutic effect of arsenic trioxide against HCC, which brings new opportunities for HCC treatment.

Methods: A pH-sensitive charge inversion material was used to construct a nano-targeted delivery system based on the synergistic effects of miR-34a and As_2O_3. We established in vitro and in vivo models of HCC microwave ablation and performed in-depth research on the dual-drug system to inhibit the rapid progression and induce pyroptosis in HCC cells after microwave ablation.

Results: The antitumour effects were enhanced with the dual-drug nanoparticles relative to the single-drug formulations, and the therapeutic efficacy of the nanoparticles was more significant in a weakly acidic environment. The dual-drug nanoparticles increased the N-terminal portion of GSDME and decreased the expression of Cyt-c and c-met.

Conclusions: Dual-drug nanoparticles may improve the therapeutic efficacy of HCC treatment after insufficient ablation through Cyt-c and GSDME-N and decrease the expression levels of c-met. These nanoparticles are expected to provide new treatment methods for residual HCC after MWA, prolong the survival of patients and improve their quality of life.

Keywords: Hepatocellular carcinoma, Microwave ablation, Nanodrug delivery, Arsenic trioxide, miR-34a

Introduction

Hepatocellular carcinoma (HCC) is one of the most common malignant tumours and is associated with rapid development and a poor prognosis (Llovet et al. 2021). Surgical treatment is inappropriate for most patients, while microwave ablation (MWA) may be

suitable for unresectable HCC (Zhang et al. 2015; Lau and Lai 2009; Zhou et al. 2017; Poulou et al. 2015; Nault et al. 2018).

MWA is effective for smaller tumours, whereas insufficient ablation leaves residual tumours that develop into larger tumours (Zhang et al. 2015). In addition, tumours adjacent to important structures are more frequently incompletely ablated in an effort to prevent damage to normal structures. Therefore, insufficient tumour ablation limits the efficacy of MWA in the clinic. Studies have shown that there are many factors contributing to the rapid progression of residual tumours after incomplete thermal ablation, such as abnormal miRNA regulatory networks, autophagy regulatory disorders and tumour-infiltrating T cell failure (Iwahashi et al. 2016; Zhao et al. 2018; Shi et al. 2019).

Abnormal expression of key miRNAs in HCC is closely related to the malignant biological behaviours of tumours, among which a low expression level of miR-34a is associated with poor prognosis of HCC. Studies have demonstrated that the expression level of miR-34a in residual tumours after ablation is downregulated (Iwahashi et al. 2016). In the pathological environment of HCC, miR-34a activation is blocked, thus leading to decreased miR-34a expression and subsequent cancer development. Restoration of the decreased levels of miR-34a may be an alternative therapy for systemic treatment of HCC. miR-34a in combination with chemicals could achieve better treatment efficacy, and this regimen has gained much attention (Hu et al. 2016; Lin et al. 2019).

In vivo, miRNAs are easily metabolized by nucleases in plasma and difficult to transport through membranes; therefore, their gene interference efficiency is low. The above problems hamper the therapeutic efficacy of miRNAs. miRNA delivery carriers depend on high binding affinity for miRNA during circulation to prevent degradation, while the rapid release of miRNA into the cytoplasm triggers gene silencing. Nanoparticles with a near neutral surface charge have favourable pharmacokinetics and biological distribution after systemic injection. Currently, there are few studies on RNA delivery systems with a nearly neutral zeta. miRNA-DSPE exhibits disulfide bonding between miRNA-DSPE in the shell that is shielded by polyethylene glycol (PEG) to prevent nuclease degradation in the physiological environment (Chan et al. 2019; Oshima et al. 2017; He et al. 2016). The combination of pH- and GSH-sensitive bonds between DSPE and other drugs is beneficial in drug delivery to control drug release and improve efficacy. Redox potential has become an effective stimulant of intracellular drug release due to the significant difference in glutathione (GSH) concentration between cancer cells and normal extracellular matrix. Moreover, the levels of GSH in cancer cells are higher than those in normal cells (Xie et al. 2020). In addition, combinations including PEGyl-based polymers are helpful for long circulation times and aggregation in tumour sites.

The main form of arsenic trioxide in water is arsenite (As(OH)3), and its trivalent arsenic exerts a key role in antitumour efficacy. Currently, arsenic trioxide is mainly loaded into liposomes (Fei et al. 2017). The tumour site is a weakly acid environment; thus, materials that display charge reversal in a weakly acidic environment could be prone to accumulate in the tumour through the EPR effect and further improve efficacy. pH-sensitive charge reversal polymers based on PAEs (poly(-amino esters)) provide effective drug delivery and also control drug release depending on the pH gradient (Chen et al. 2015, 2018; Yu et al. 2014; Ramos et al. 2014).

This research aimed to construct a nanodelivery system with synergistic effects caused by carrying both As_2O_3 and miR-34a to inhibit tumour progression after MWA. The nanodelivery system was prepared using an amphiphilic triblock copolymer (mPEG-PLA-PAE), miR-34a-DSPE, mPEG-DSPE and arsenic trioxide using the double emulsion method. Hydrophilic mPEG fragments form protective shells on the outside of the nanoparticles, thus providing a stable drug delivery system and extending the circulation time in the body. Hydrophobic PAE segments (pH > pKa) contribute to increased micelle stability, and hydrophilic PAE segments with a high positive potential (pH < pKa) can increase cell internalization and uptake. We used sublethal cancer cells to mimic insufficient ablation to conveniently detect the efficacy of this system. We believe that these particles hold great promise for clinical translation to inhibit the progression of HCC ablation.

Materials and methods

mPEG-PLA-PAE was obtained from Xi'an Ruixi Biotechnology Co., Ltd. DSPE-PDP was purchased from Shanghai Langxu Biotechnology Co., Ltd. mPEG-DSPE was provided by Shanghai Fansuo Biotechnology Co. Ltd. Arsenic trioxide was kindly provided by the Chinese Academy of Sciences. RIPA lysis buffer was purchased from Beyotime Institute of Biotechnology. Monoclonal antibodies against c-met, GSDME and Cyt-c were obtained from Abcam. Monoclonal antibodies against GAPDH and caspase-3 were purchased from Cell Signalling Technology. β-Actin–HRP were obtained from Proteintech.

Preparation of the As/miR-34a-mPEG-PLA-PAE nanoparticles

mPEG-PLA-PAE NPs were prepared as previously described. As/miR-34aNPs (As/miR-34a-mPEG-PLA-PAE nanoparticles) were prepared by a double emulsion method as follows. miR-34a-SH was conjugated to DSPE-PDP as previously reported. Briefly, a 0.1 ml aqueous solution of As_2O_3 (1 mg/ml) and 0.2 ml of a DSPE-miR34a (0.125 μmol/ml) solution were emulsified in 0.5 ml of dichloromethane containing 20 mg of mPEG-PLA-PAE and 4 mg of mPEG-DSPE (PEG-modified phospholipid) using an ultrasonic processor at 400 W for 2 min. Next, the water/oil (w/o) emulsion was added to 1.7 ml of a Pluronic F68 water solution (1 mg/ml) and the mixture was sonicated at 400 W for 2 min. Subsequently, the resulting w/o/w emulsion was stirred at room temperature to evaporate the organic phase.

Characterization of the nanoparticles

The morphology of nanoparticle at pH 7.4 and pH 6.5 was observed by transmission electron microscopy (TEM). The nanoparticles potentials at different acidities (pH = 7.4, 6.5, 5.5) was determined with a Nano-ZS analyser. As/miR-34aNPs were incubated with GSH at pH 7.4 or pH 6.5, and the DNA gel block method was then used to determine miRNA stability after serum incubation. The film dialysis method was used to measure the amount of the drug released at different time points to evaluate drug release properties as described in a previous report. Inductively coupled plasma mass spectrometry (ICP-MS) was used to determine the encapsulation efficiency and drug loading of As_2O_3 (As) according to a previous procedure.

Sublethal heat treatment of the HCC cell lines as an insufficient microwave ablation model

Huh7, PLC/PRF/5, and Hep1–6 cells at a density of 5×10^5 cells/cm^3 were inoculated into DMEM containing 10% foetal bovine serum (FBS) and cultured (37 °C) overnight. Then, they were treated at 47 °C for 10 min. After heating, the DMEM was replaced three times a day until the 3rd day to remove debris and dead cells. Then, the cell number was adjusted to 1×10^6/cm^3 on the 5th day after heating, the surviving HCC cells were subcultured in new culture dishes, and these cell lines were named H-Huh7, H-PLC, and H-Hep1–6. This procedure was performed three times. c-met expression was detected by Western blot analysis. H-Huh7, H-PLC, and H-Hep1–6 cells at 5×10^3 cells/cm^3 in 96-well plates were cultured overnight according to a procedure similar to that used for to study viability using the MTT method. As_2O_3 and miR-34a (according to the reagent procedure) were applied using the same methods for determining cell viability and c-met expression. Different concentrations of blank nanoparticles were added to LO2 human liver cells to determine viability using the MTT method.

As/miR-34aNPs inhibition of the growth of HCC cell lines subjected to sublethal heat treatment

H-Huh7, H-PLC, and H-Hep1–6 cells were inoculated into 96-well plates at a fusion rate of approximately 50%. PBS, miR-34aNPs and AsNPs (As_2O_3NPs) were added for culture at pH 7.4 for 48 h. As/miR-34aNPs were added at pH 6.5 and pH 7.4. Finally, MTT was added, and the cells were cultured for an additional 4 h.

Cellular uptake of nanoparticles by H-Huh7 and H-PLC cells

Cy3-labelled nanoparticles were prepared according to the above procedure. Cy3NPs and free cy3 were inoculated into H-Huh7 and H-PLC cells in a normal physiological environment. Cy3NPs were inoculated into H-Huh7 and H-PLC cells at pH 6.5, further verifying that the acid-sensitive charge reversal mechanism was beneficial for cellular uptake, which was observed by confocal microscopy.

Antitumour mechanisms of As/miR-34aNPs in vitro

H-Huh7, H-PLC, and H-Hep1-6 cells were inoculated into 6-well plates at a fusion rate of approximately 50%. PBS, miR-34aNPs and AsNPs (As_2O_3NPs) were added for culture at pH 7.2 for 48 h. As/miR-34aNPs were added at pH 6.5 and pH 7.2. The expression of C-met, caspase-3, GSDME, Cyt-c, and cell medium Cyt-c was assessed by Western blot. The LDH release was determined according to the protocol of Promega.

As/miR34aNPs triggering of Cyt-c release

HEK293T cells were transiently transfected with GSN-GFP or GSC-GFP and then observed by fluorescence microscopy after treatment with As_2O_3 for 24 h. GSN-mCherry and GSC-mCherry were also transiently transfected into HEK293T cells. Then, mitochondria and mCherry were observed by confocal microscopy, MitoTracker (Green) was used to stain the mitochondria, and Hoechst 33342 was

used to indicate the nuclei. H-Huh7 cells were treated for 48 h with PBS, AsNPs and miR34aNPs at pH 7.4 and As/miR34aNPs at pH 7.4 and 6.5. The expression levels of Cyt c (cytochrome C) and Cyt c in the culture media (s-Cyt c) were assessed by Western blot analysis.

Cellular uptake of the nanoparticles in vivo

Six-week-old BALB/c female nude mice were obtained from Slack Laboratory Animal Co., Ltd. (Shanghai, China). All animal experimental procedures were carried out according to protocols approved by the Animal Care and Use Committee of Shenzhen People's Hospital. An insufficient microwave ablation HCC model was established by subcutaneous inoculation of the sublethal heat-treated HCC cell line H-Huh7 into the nude mice. When the tumour grew to a size of 200 mm^3, Cy3NPs were administered to the mice via the tail vein and the mice were sacrificed after 48 h. Tumour sections were prepared to observe the fluorescence distribution by confocal microscopy.

Antitumour therapy in an insufficient microwave ablation model

An H-Huh7 suspension was inoculated into the right backs of mice to establish a subcutaneous transplanted tumour model. When the tumours grew to 200 mm^3, the mice were randomly divided into four groups with six mice per group. All miR-34a formulations were equivalent to 125 nmol/kg body weight, and As_2O_3 formulations were equivalent to 0.5 mg/kg body weight. All formulations were intravenously administered once a week. Tumour growth was monitored and recorded with callipers eight times over three weeks. The tumour volume (V) was calculated based on the following formula: $V = [\text{major axis}(\text{minor axis})^2]/2$. Then, the mice were sacrificed and the tumours were excised and photographed. To evaluate the potential cytotoxicity of the formulations in vivo, at the end of the treatment, serum biochemical analysis was performed. Liver function was estimated by the serum levels of ALT, AST, and ALP. Kidney function was verified based on the serum levels of BUN and CRE.

Statistical analysis

All values are presented as the mean ± SD. Statistical significance was determined by one-way analysis of variance using SPSS software (version 17.0, IBM Inc., Chicago, IL, USA). Differences were considered significant at $p < 0.05$ and highly significant at $p < 0.01$.

Results

Development of a sublethal heat treatment model to mimic insufficient microwave ablation of HCC

First, heat treatment methods was performed to mimic insufficient MWA of HCC. Cell growth after incubation for 48 h was examined by MTT assay. H-PLC and H-huh7 cells grew more rapidly than the wild-type cells (Fig. 1A). Western blotting was performed to detect the changes in c-met expression after sublethal treatment. c-met was upregulated in both cell types. Then, miRNA was added to regulate the related gene expression. c-met was downregulated after treatment with miR34a for 48 h (Fig. 1B). The results showed that compared with As or miR34a alone, the survival rates of H-huh7 and

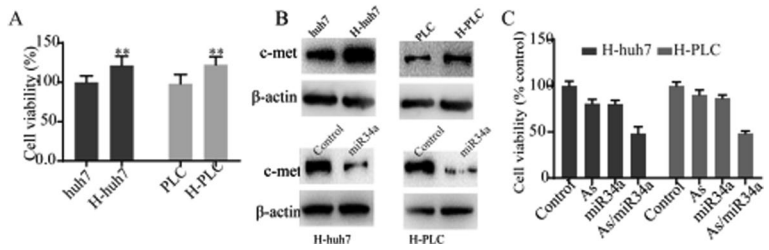

Fig. 1 Insufficient microwave ablation of HCC. **A** Cell viability of Huh7 and PLC cells after three incubations at 47 °C for 10 min each time. The corresponding residual cells were named H-Huh7 and H-PLC. **B** Upper panel: c-met expression in H-huh7 and H-PLC cells was assessed by Western blot analysis. Lower panel: H-huh7 and H-PLC cells were treated with miR-34a. **C** Cell viability of H-huh7 and H-PLC cells after treatment with As_2O_3(As), miR34a and their combination. $^*p < 0.05$, $^{**}p < 0.01$ compared with the control

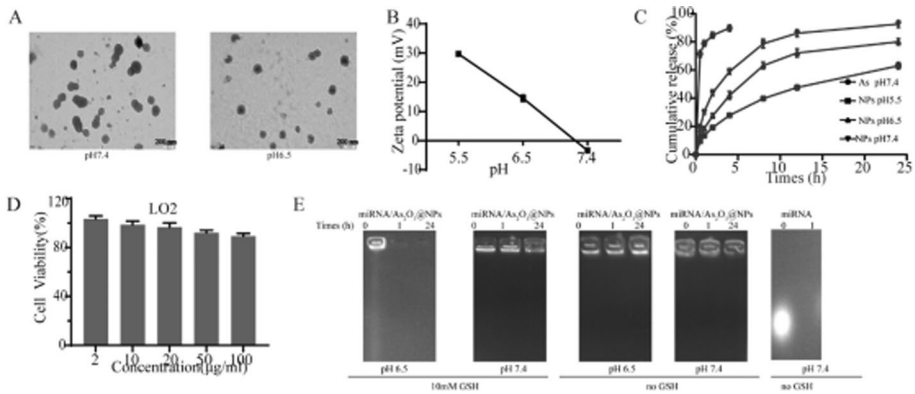

Fig. 2 Characteristics of the As/miR34aNPs. **A** TEM images under different pH conditions. **B** Zeta potentials of As/miR34aNPs measured by DLS at different pH values. **C** Cell viability after treatment with blank nanoparticles was examined by MTT assay. **D** Drug release curves (pH 7.4 or pH 6.5, with or without GSH treatment). **E** miRNA agarose gel electrophoresis experiment. As/miR34aNPs were incubated with serum at different pH values for 24 h (pH 7.4 or pH 6.5, with or without GSH treatment)

H-PLC in the As/miR34a groups were significantly lower. The As/miR-34a groups had better antiproliferative effects than the single-formulation groups, indicating that combination treatment may have a stronger antitumour effect (Fig. 1C). A previous report indicated that As_2O_3 triggers pyroptosis and induces GSDME cleavage (Additional file 1: Fig. S1).

Characterization of the As/miR34a@NPs

The morphology of the nanoparticles was observed by TEM. As shown in Fig. 2A, the nanoparticles were small and nearly spherical with good dispersion. At physiological (pH 7.4), the size of NPs was approximately 150 nm. At pH 6.5, the average particle size decreased to 110 nm. As shown in Fig. 2B, nanoparticles under normal physiological conditions showed a negative charge that shifted to a positive charge at pH 6.5, and arsenic was rapidly released in the slightly acidic environment (Fig. 2B, C). These results suggested that the drug delivery system has the potential to increase drug accumulation at tumour sites with long circulation time while increasing drug uptake in weakly acidic environments with charge reversal.

The release characteristics of the miRNA were similar to those of arsenic trioxide. These formulations slowed the degradation of miRNA in serum, and the miRNA was released rapidly under the action of 10 mM GSH (Fig. 2E). The acid sensitivity of these NPs contributes to their accumulation in tumour tissues through the EPR effect in circulation. Drug safety is an important aspect that must be evaluated to determine the potential clinical use of new therapies. The normal cell line LO2 has been widely used to detect toxicity. The viability of LO2 cells after treatment with blank nanoparticles for 48 h indicated that the blank nanoparticles had low toxicity to normal cells (Fig. 2D).

Cell uptake of NPs in insufficient ablation cells

Effective uptake of chemicals can be beneficial to achieving good antitumour efficacy. Generally, ensuring that most of the drug enters the cancer cell leads to better antitumour activity. In this section, the cellular uptake of the nanocarriers was examined by confocal microscopy. Compared with free miR-Cy3, the fluorescence intensity of the miR-Cy3-NPs was stronger at pH 7.4. In a more acidic environment (pH 6.5), the intensity of the NPs was enhanced due to charge inversion (Fig. 3). This finding indicates that the charge inversion of the nanoparticles induced by the pH alteration effectively promoted chemical uptake. The uptake of drugs could therefore be enhanced under slightly acidic conditions.

As/miR34aNPs trigger insufficient ablation cell pyroptosis

Cells with large bubbles that also release LDH are recognized as the key features of cells undergoing pyroptosis. As/miR34aNP treatment induced the formation of the characteristic large bubbles from the plasma membrane of dying cells and whole cells, which is characteristic of typical swelling. However, cells with pyroptosis features induced by As/miR34aNPs at pH 6.5 were more obvious than those at pH 7.4 (Fig. 4A, Additional file 1: Fig. S2). Moreover, LDH release induced by the combination treatment was more profound than that induced by the single formulation, and LDH release was greater in an acidic environment (Fig. 4B, C). To evaluate the inhibitory effects of the drug-loaded nanoparticles on the proliferation of sublethal cells, an MTT assay was used to evaluate the proliferation of H-Huh7 and H-PLC cells. The results showed that compared with the single formulations, the survival rates of H-Huh7 and H-PLC cells after treatment

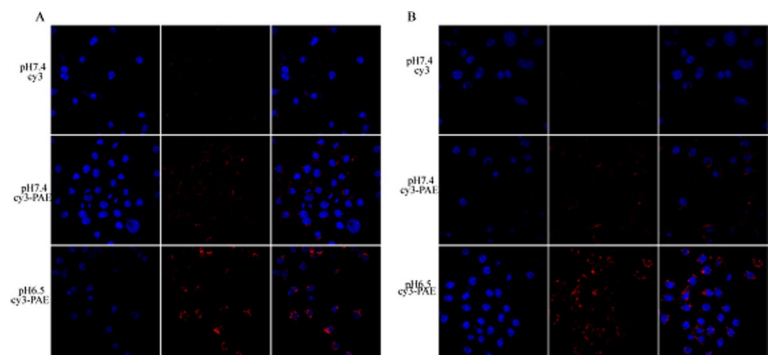

Fig. 3 **A** Cellular uptake of the nanocarriers by H-Huh7 cells observed by confocal microscopy. **B** Cellular uptake of the nanocarriers by H-PLC cells observed by confocal microscopy

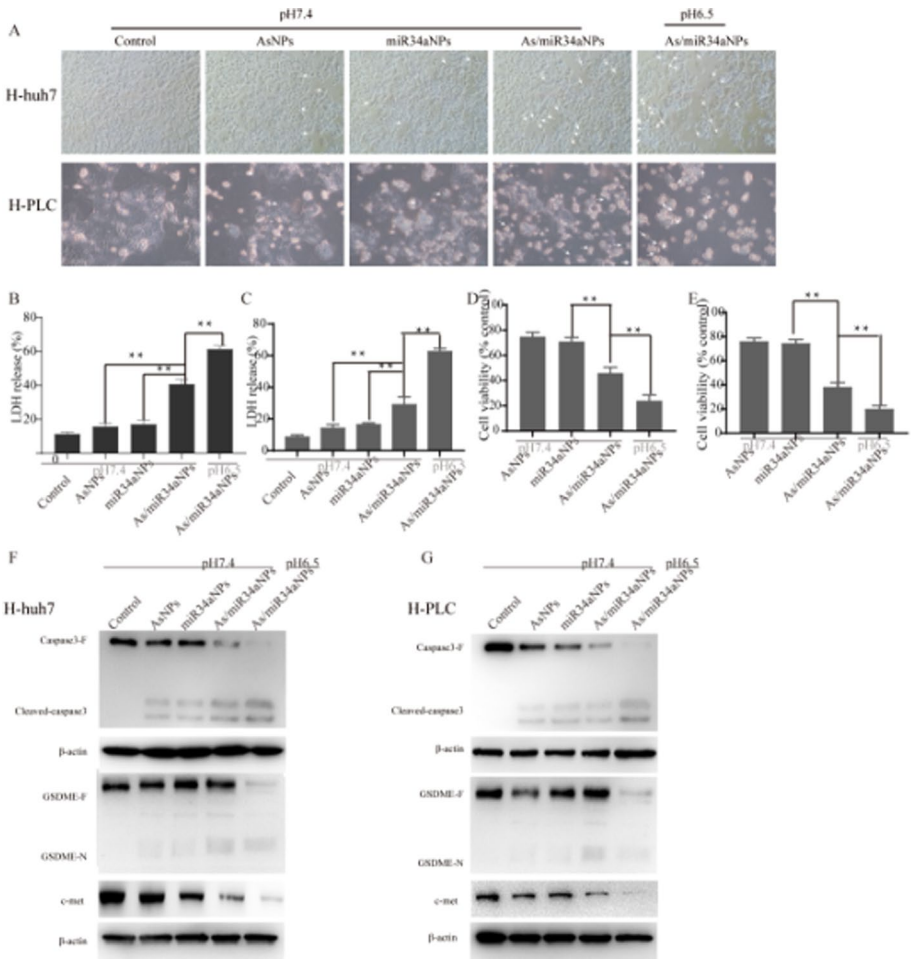

Fig. 4 As/miR34aNPs induced sublethal HCC pyroptosis. **A** Representative microscopic images of H-Huh7 and H-PLC cells treated with PBS, AsNPs and miR34aNPs in a normal physiological environment and As/miR34aNPs in normal and acidic environments. White arrowheads indicate the characteristic bubbles in the cell membrane (×400). **B**, **C** LDH release was assessed to measure cell membrane destruction. **D**, **E** Cell viability was detected by the MTT method. **F**, **G** The expression levels of caspase-3, GSDME, c-met and β-actin were assessed by Western blot analysis. $^{*}p < 0.05$, $^{**}p < 0.01$ compared with the control

with As/miR34aNPs were significantly lower, indicating that the combined treatment may have a stronger antitumour effect. In a slightly acidic environment, the combined treatment exerted a significant therapeutic effect (Fig. 4D, E). The charge reversal ability of the As/miR34aNPs renders them an ideal nanodelivery carrier to maximize the therapeutic efficacy by inducing pyroptosis.

GSDME is another member of the gasdermin family. This protein has a gasdermin-N domain similar to that of GSDMD and can induce pyroptosis in cancer cells with expressing GSDME. GSDME is a key determining protein of H-Huh7 and H-PLC cells undergoing pyroptosis induced by arsenic trioxide. The levels of the GSDME-F and GSDME-N proteins were assessed by Western blot analysis for 48 h in HCC cells after drug treatment. The results showed that the drug-loaded nanoparticles increased the proportion of the N-terminal part of GSDME, while the antitumour efficacy of the dual-drug nanoparticles in the weakly acidic environment was more significant (Fig. 4F,

G). The expression of GSDME-N and cleaved caspase-3 increased after treatment with As/miR34aNPs (Additional file 1: Fig. S3). c-met is closely related to the prognosis of tumour patients. The results showed that the dual drug-loaded nanoparticles reduced the expression levels of c-met and the effect of the nanoparticles was more significant in the weakly acidic environment.

As/miR34aNPs triggered Cyt c release

The GSDME-N portion was expressed at low levels under normal conditions; however, its expression was higher after treatment with chemicals. HEK293T cells were treated with As_2O_3 after transient transfection with GSDME-N-GFP. The fluorescence intensity after As treatment in Fig. 5A was brighter than that of the control group. However, the intensity of GSC-GFP-transfected cells after treatment with As was almost unchanged (Fig. 5A). We observed overlap between GSDME-N mCherry puncta and MitoTracker Green-stained mitochondria in GSDME-N-EGFP-expressing HEK293T cells (Fig. 5B). Similar results were observed for the GSDME-C portion. In previous results, GSDME-N targeted the mitochondria to release the death protein Cyt c. In this analysis, we found that As_2O_3 treatment may enhance GSDME-N stability to trigger additional Cyt c release. Cyt c release induced by the combination treatment was more profound than that induced by the single formulations, and its triggered release occurred at a higher level in an acidic environment (Fig. 5C).

Combination therapy inhibited the HCC progression after insufficient ablation in vivo

To estimate the use of the dual-drug formulation as a potential therapy to inhibit the progression after insufficient MWA, sublethal HCC cells were used as an insufficient MWA cell model according to a previous procedure. An in vivo antitumour efficacy

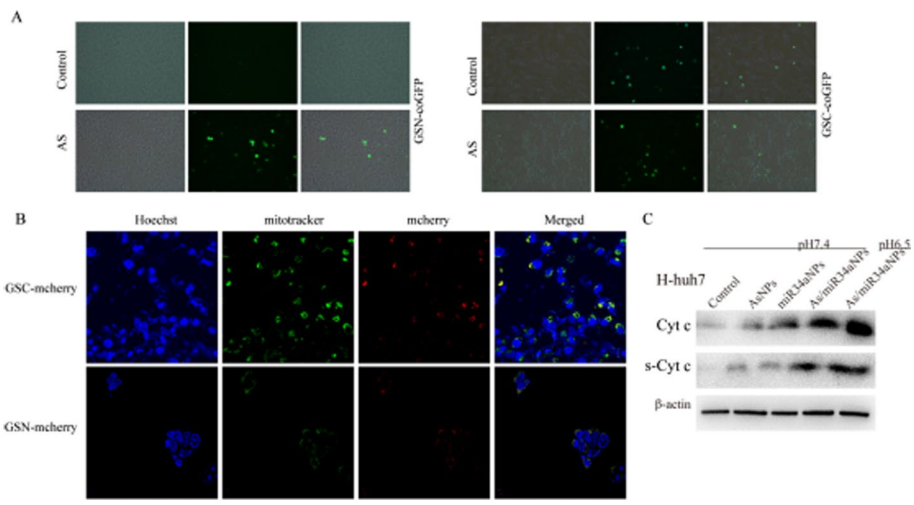

Fig. 5 As/miR34aNPs triggered Cyt c release. **A** Representative microscopic images of HEK293T cells treated with As_2O_3 after transient transfection with GSN-GFP or GSC-GFP. **B** GSN-mCherry and GSC-mCherry were transiently transfected into HEK293T cells. Then, the mitochondria and mCherry were observed by confocal microscopy, MitoTracker was used to stain the mitochondria, and Hoechst 33342 was used to mark the nuclei. **C** H-Huh7 cells were treated for 48 h with PBS, AsNPs and miR34aNPs in a normal physiological environment and As/miR34aNPs in a normal and acidic environment. The expression levels of Cyt c and Cyt c in the culture media (s-Cyt c) were examined by Western blot analysis

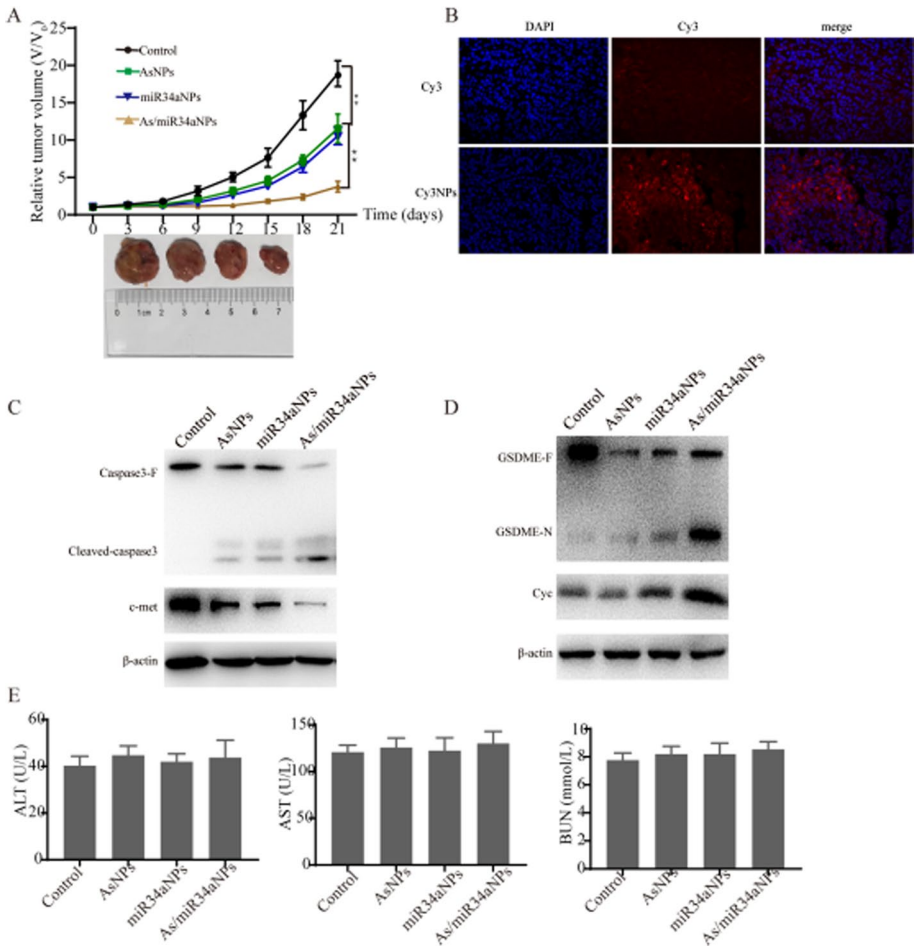

Fig. 6 In vivo antitumour performance of different formulations in H-Huh7 tumour-bearing nude mice. **A** Tumour growth curves of different groups after treatment with the four formulations (control, AsNPs, miR34aNPs and As/miR34aNPs). Data are shown as the mean ± S.D. ($n = 6$). *$p < 0.05$, **$p < 0.01$ compared with the control. **B** Intratumoural fluorescence of Cy3-labelled miRNA (red) visualized by CLSM 24 h post-injection. The nucleus is stained with DAPI (blue). **C**, **D** Expression levels of GSDME, c-met, and Cyt-c in vivo were assessed by Western blot analysis. **E** Levels of alanine aminotransferase (ALT), aspartate aminotransferase (AST) and blood urea nitrogen (BUN) were assessed to evaluate the side effects of the different formulations after in vivo treatment

study was performed using a subcutaneous H-Huh7 cell-derived xenograft mouse model. The effective concentration of drugs in the tumours and the drug uptake by tumour cells are key to the effectiveness of anticancer treatments. We used Cy3 to trace the nanoparticles after i.v. injections. Cy3-labelled nanoparticles showed higher intratumoural accumulation than Cy3 alone (Fig. 6B), which was confirmed by fluorescence measurements in tumour samples. We further investigated the antitumour activity of As/miR34aNPs in vivo. When the tumour sizes reached approximately 200 mm^3, the H-huh7 tumour-bearing nude mice were divided into four groups and treated with different i.v. injections: control, AsNPs, miR34aNPs and As/miR34aNPs. Then, the tumour volumes were measured and plotted every 3 days (Fig. 6A). The results showed that in the PBS-treated group, the tumours grew rapidly, whereas in

the single-formulation groups, effective tumour suppression was observed that was better than that of the control group. However, the As/miR34aNP treatment exhibited greater antitumour efficacy than the single formulations. As/miR34aNPs increased c-met, Cyt-c, and cleaved caspase-3 levels and the N-terminal proportion of GSDME (Fig. 6C, D). To evaluate the potential cytotoxicity of the formulations in vivo, serum biochemical analysis was performed. Liver function was estimated by the serum levels of aminotransferase (ALT), aspartate aminotransferase (AST), and alkaline phosphatase (ALP). Kidney function was verified with serum blood urea nitrogen (BUN) and creatinine (CRE) evaluation. Nonsignificant changes in the biochemical indices in the four formulation groups indicated that this nanomedicine exhibits few side effects, suggesting its good biosafety in vivo (Fig. 6E, Additional file 1: Fig. S4).

Discussion

Insufficient heat therapy, such as MWA, can lead to the aggressive progression and rapid growth of residual tumours. Traditional treatment, such as chemotherapy, can prevent the progression of residual tumour cells. The miRNA regulatory network is abnormal after thermal ablation of tumours, in which miR34a expression decreased. Low expression of miR34a is closely related to poor prognosis, and miR34a supplementation can lower the dosage of other chemicals required to inhibit tumour growth. miR34a combined with As_2O_3 can reduce c-met protein expression, which is of positive significance for MWA therapy and may be used as a potential candidate clinical treatment.

The use of arsenic trioxide to treat acute promyelocytic leukaemia has progressed, as have treatments for other tumours. Arsenic trioxide has several antitumour mechanisms, G2/M phase arrest and apoptosis and inhibition of invasion and migration have been well investigated (Zhang et al. 2012; Wang et al. 2019). Investigating the novel antitumour mechanisms of these chemicals may be beneficial for improving therapy. In this study, we found that miR34a could sensitize arsenic trioxide to trigger pyroptosis. The removal of arsenic trioxide and its products from the blood by the reticuloendothelial system prevents a therapeutic dose from accumulating at the site of the tumour. To overcome this obstacle, arsenic trioxide and other arsenic compounds have been successfully loaded into polymer vesicles, liposomes, and other nanoparticles. To inhibit or eradicate residual cancer cells, nanoparticles have been widely used as carriers to deliver drugs with sustained release characteristics. However, miRNAs are prone to rapid degradation by nucleases in plasma in vivo, and they show weak transport abilities across cell membranes, short half-lives and low gene interference rates. These obstacles hinder miRNA antitumour efficacy and limit further research. In this study, we used DSPE as a skeleton onto which chemicals were loaded. The combination of pH- and GSH-sensitive bonds between DSPE and the drugs is beneficial for controlling drug release during delivery and improving efficacy.

If nanocarriers or drugs resist entering tumour cells, their ability to kill tumour cells will be greatly limited. pH-sensitive charge inversion polymers based on PAEs (poly(amino ester)) have effective drug delivery capacities to trigger drug release depending on the pH gradient. PEG-based nanodelivery systems facilitate a long circulation time in the body, thereby increasing PEG-based nanocarrier accumulation at tumour sites. The nanocarrier can more easily enter cells than the free drug, and the

uptake of the nanocarrier can be enhanced in the weakly acidic tumour environment, which can be beneficial to effectively inhibit tumour growth and reduce side effects.

Cell death in all multicellular organisms plays an important role in growth, survival and homeostasis. Pyroptosis is induced by chemicals, toxic agents and even viral infection and represents a novel form of cell death that has been discovered in recent years. Pyroptosis has the characteristics of membrane pore formation, with typical swelling and cytoplasmic content release. In this study, As/miR34aNPs generated more cells that showed the swelling and bubble formation typical of pyroptosis. GSDMD has been demonstrated to play a key role in membrane pore formation and triggers pyroptosis during inflammatory caspase-1/-11/-4/-5 activation (Shi et al. 2015). GSDME is another member of the gasdermin superfamily similar to GSDMD. It has the same function as GSDMD during the formation of membrane pores. GSDME activation triggers pyroptosis in cells with high GSDME expression after chemical treatment (Rogers et al. 2017, 2019; Wang et al. 2017). The GSDME gene is inactivated by epigenetic mechanisms in many types of cancer, including colorectal, stomach and breast cancer. Currently, there are few studies on liver cancer cell pyroptosis. HepG2 cells express the GSDME protein, form GSDME-N fragments after cytochrome C treatment and cause pyroptosis (Rogers et al. 2017). In a previous report, GSDME-N was found to be released into the cell plasma and mitochondria. We discovered that both GSDME-N and GSDME-C could reside in mitochondria. GSDME cleavage is triggered by caspase-3 activation after treatment with chemicals. GSDME-N is released to the membrane and mitochondria. Drug treatment stabilized GSDME-N and triggered Cyt-c release and then cleaved GSDME indirectly to form a loop (Fig. 7). Dual-drug nanoparticles induced pyroptosis characteristics in more cells, while the ratio of GSDME-N/GSDME increased, indicating that dual-drug nanoparticles may improve therapeutic efficacy against HCC with after insufficient ablation through GSDMD-N.

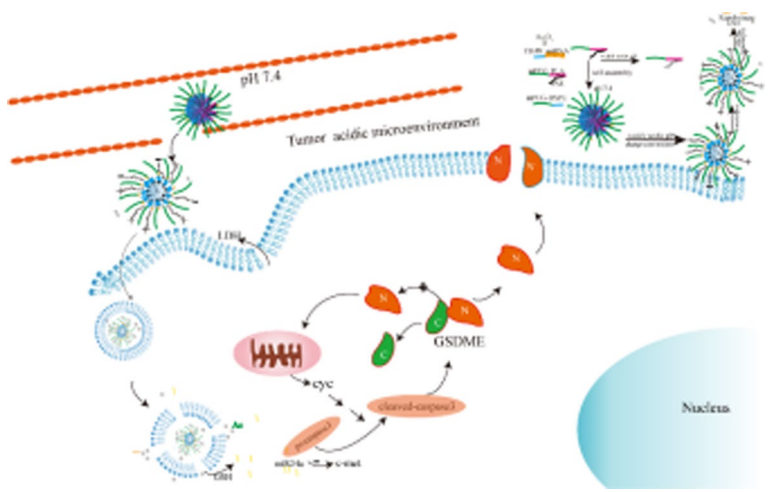

Fig. 7 As/miR34aNPs inhibits the HCC progression after insufficient ablation in vivo. As/miR34aNP uptake by tumour cells was enhanced in the slightly acidic tumour microenvironment. This formulation could inhibit c-met expression to exert antitumour efficacy. GSDME cleavage is triggered by caspase-3 activation after treatment with As/miR34aNPs. GSDME-N is released into the membrane and mitochondria. Drug treatment stabilized GSDME-N and triggered Cyt-c release and then cleaved GSDME indirectly to form a loop

Conclusion

A novel nanoplatform with a synergistic combined strategy was designed that showed effective therapeutic efficacy to prevent the progression of HCC after insufficient ablation. The drug carriers showed good biocompatibility and could be taken up by tumour cells in the slightly acidic tumour microenvironment. Drug treatment may stabilize GSDME-N, which triggers Cyt-c release. These dual drug-loaded nanoparticles may improve antitumour therapy by downregulating c-met expression, upregulating Cyt-c expression and increasing the GSDME-N ratio. We believe that this novel combined therapy approach may be a promising avenue in the field of MWA.

Abbreviations

GSDME-N: The N-terminal proportion of GSDME; GSDME-C: The C-terminal proportion of GSDME; As: Arsenic trioxide.

Supplementary Information

The online version contains supplementary material available at https://doi.org/10.1186/s12645-021-00105-8.

Additional file 1: Fig. S1. Arsenic trioxide reduced c-met expression and triggered GSDME activation. (A–C) Cells were treated with increasing doses of arsenic trioxide as previously described. Then, the expression of c-met and GSDME was detected by western blot. **Fig. S2.** Drug Formulations could induce pyroptosis of H-Hep1-6. (A) Representative microscopy images of H-Hep1-6 treated with PBS, AsNPs and miR34aNPs in a normal physiological environment and As/miR34aNPs in a normal and acidic environment. Blank arrowheads indicate the characteristic bubbles in the cell membrane (400×). (B) c-met and GAPDH were detected by western blot. **Fig. S3.** Expression of GSDME and caspase in cell medium. The expression levels of caspase3 and GSDME in the medium were detected by western blot as described in Fig. 4. **Fig. S4.** The safety evaluation of the formulations. (A) The levels of creatinine and ALP were detected to evaluate the side effects of different formulations in vivo after the treatment.

Acknowledgements

Not applicable.

Authors' contributions

JH performed the experiments. WCP helped with data analysis, and data interpretation. JH, ZYJ, ZHL designed research, revised and finalized the manuscript. All authors read and approved the final manuscript.

Funding

This work was supported by the National Natural Science Foundation (81903161), Shenzhen's Natural Science Foundation-Basic Research Project (JCYJ20210324113811032, 20210318132025), China postdoctoral science foundation (2019M663397).

Availability of data and materials

All remaining data are available within the article and supplementary files, or available from the authors upon request.

Declarations

Ethics approval and consent to participate

The study was authorized by the Ethic Committee of Shenzhen People's Hospital. Written informed consent was provided from each subject. All animal experimental procedures were carried out according to protocols approved by the Animal Care and Use Committee.

Consent for publication

All authors have agreed to publish this manuscript.

Competing interests

The authors declare no competing financial interests.

Author details

[1]Department of Oncology Radiotherapy, The Second Clinical Medical College, Jinan University (Shenzhen People's Hospital), Shenzhen 518020, China. [2]Integrated Chinese and Western Medicine Postdoctoral Research Station, Jinan University, Guangzhou 510632, China. [3]Department of Microbiology and Immunology, College of Basic Medicine and Public Hygiene, Jinan University, Guangzhou 510632, China. [4]Department of Gastroenterology, Civil Aviation Hospital of Shanghai, Shanghai, China.

Received: 11 July 2021 Accepted: 8 November 2021
Published online: 27 November 2021

References

Chan C, Guo N, Duan X, Han W, Xue L, Bryan D, Wightman SC, Khodarev NN, Weichselbaum RR, Lin W (2019) Systemic miRNA delivery by nontoxic nanoscale coordination polymers limits epithelial-to-mesenchymal transition and suppresses liver metastases of colorectal cancer. Biomaterials 210:94–104

Chen F, Zhang J, Wang L, Wang Y, Chen M (2015) Tumor pH(e)-triggered charge-reversal and redox-responsive nanoparticles for docetaxel delivery in hepatocellular carcinoma treatment. Nanoscale 7(38):15763–15779

Chen Y, Zhang L, Liu Y, Tan S, Qu R, Wu Z, Zhou Y, Huang J (2018) Preparation of PGA-PAE-micelles for enhanced antitumor efficacy of cisplatin. ACS Appl Mater Interfaces 10(30):25006–25016

Fei W, Zhang Y, Han S, Tao J, Zheng H, Wei Y, Zhu J, Li F, Wang X (2017) RGD conjugated liposome-hollow silica hybrid nanovehicles for targeted and controlled delivery of arsenic trioxide against hepatic carcinoma. Int J Pharm 519(1–2):250–262

He C, Poon C, Chan C, Yamada SD, Lin W (2016) Nanoscale coordination polymers codeliver chemotherapeutics and siRNAs to eradicate tumors of cisplatin-resistant ovarian cancer. J Am Chem Soc 138(18):6010–6019

Hu Q, Wang K, Sun X, Li Y, Fu Q, Liang T, Tang G (2016) A redox-sensitive, oligopeptide-guided, self-assembling, and efficiency-enhanced (ROSE) system for functional delivery of microRNA therapeutics for treatment of hepatocellular carcinoma. Biomaterials 104:192–200

Iwahashi S, Shimada M, Utsunomiya T, Imura S, Morine Y, Ikemoto T, Takasu C, Saito Y, Yamada S (2016) Epithelial-mesenchymal transition-related genes are linked to aggressive local recurrence of hepatocellular carcinoma after radiofrequency ablation. Cancer Lett 375(1):47–50

Lau WY, Lai EC (2009) The current role of radiofrequency ablation in the management of hepatocellular carcinoma: a systematic review. Ann Surg 249(1):20–25

Lin F, Wen D, Wang X, Mahato RI (2019) Dual responsive micelles capable of modulating miRNA-34a to combat taxane resistance in prostate cancer. Biomaterials 192:95–108

Llovet JM, Kelley RK, Villanueva A, Singal AG, Pikarsky E, Roayaie S, Lencioni R, Koike K, Zucman-Rossi J, Finn RS (2021) Hepatocellular carcinoma nature reviews. Dis Primers 7(1):6

Nault JC, Sutter O, Nahon P, Ganne-Carrié N, Séror O (2018) Percutaneous treatment of hepatocellular carcinoma: state of the art and innovations. J Hepatol 68(4):783–797

Oshima G, Guo N, He C, Stack ME, Poon C, Uppal A, Wightman SC, Parekh A, Skowron KB, Posner MC, Lin W, Khodarev NN, Weichselbaum RR (2017) In vivo delivery and therapeutic effects of a MicroRNA on colorectal liver metastases. Mol Ther 25(7):1588–1595

Poulou LS, Botsa E, Thanou I, Ziakas PD, Thanos L (2015) Percutaneous microwave ablation vs radiofrequency ablation in the treatment of hepatocellular carcinoma. World J Hepatol 7(8):1054–1063

Ramos J, Potta T, Scheideler O, Rege K (2014) Parallel synthesis of poly(amino ether)-templated plasmonic nanoparticles for transgene delivery. ACS Appl Mater Interfaces 6(17):14861–14873

Rogers C, Fernandes-Alnemri T, Mayes L, Alnemri D, Cingolani G, Alnemri ES (2017) Cleavage of DFNA5 by caspase-3 during apoptosis mediates progression to secondary necrotic/pyroptotic cell death. Nat Commun 8:14128

Rogers C, Erkes DA, Nardone A, Aplin AE, Fernandes-Alnemri T, Alnemri ES (2019) Gasdermin pores permeabilize mitochondria to augment caspase-3 activation during apoptosis and inflammasome activation. Nat Commun 10(1):1689

Shi J, Zhao Y, Wang K, Shi X, Wang Y, Huang H, Zhuang Y, Cai T, Wang F, Shao F (2015) Cleavage of GSDMD by inflammatory caspases determines pyroptotic cell death. Nature 526(7575):660–665

Shi L, Wang J, Ding N, Zhang Y, Zhu Y, Dong S, Wang X, Peng C, Zhou C, Zhou L, Li X, Shi H, Wu W, Long X, Wu C, Liao W (2019) Inflammation induced by incomplete radiofrequency ablation accelerates tumor progression and hinders PD-1 immunotherapy. Nat Commun 10(1):5421

Wang Y, Gao W, Shi X, Ding J, Liu W, He H, Wang K, Shao F (2017) Chemotherapy drugs induce pyroptosis through caspase-3 cleavage of a gasdermin. Nature 547(7661):99–103

Wang HY, Zhang B, Zhou JN, Wang DX, Xu YC, Zeng Q, Jia YL, Xi JF, Nan X, He LJ, Yue W, Pei XT (2019) Arsenic trioxide inhibits liver cancer stem cells and metastasis by targeting SRF/MCM7 complex. Cell Death Dis 10(6):453

Xie X, Peng Z, Hua X, Wang Z, Deng K, Yang X, Huang H (2020) Selectively monitoring glutathione in human serum and growth-associated living cells using gold nanoclusters. Biosens Bioelectron 148:111829

Yu Y, Zhang X, Qiu L (2014) The anti-tumor efficacy of curcumin when delivered by size/charge-changing multistage polymeric micelles based on amphiphilic poly(β-amino ester) derivates. Biomaterials 35(10):3467–3479

Zhang X, Jia S, Yang S, Yang Y, Yang T, Yang Y (2012) Arsenic trioxide induces G2/M arrest in hepatocellular carcinoma cells by increasing the tumor suppressor PTEN expression. J Cell Biochem 113(11):3528–3535

Zhang NN, Lu W, Cheng XJ, Liu JY, Zhou YH, Li F (2015) High-powered microwave ablation of larger hepatocellular carcinoma: evaluation of recurrence rate and factors related to recurrence. Clin Radiol 70(11):1237–1243

Zhao Z, Wu J, Liu X, Liang M, Zhou X, Ouyang S, Yao J, Wang J, Luo B (2018) Insufficient radiofrequency ablation promotes proliferation of residual hepatocellular carcinoma via autophagy. Cancer Lett 421:73–81

Zhou Q, Wu S, Gong N, Li X, Dou J, Mu M, Yu X, Yu J, Liang P (2017) Liposomes loading sodium chloride as effective thermo-seeds for microwave ablation of hepatocellular carcinoma. Nanoscale 9(31):11068–11076

Publisher's Note